

Balancing ACT: weighing prior dependency and global tensions of DR6 lensing with other datasets

A.N. Ormondroyd,^{1,2*} W.J. Handley,^{1,2} M.P. Hobson¹ and A.N. Lasenby^{1,2}

¹*Astrophysics Group, Cavendish Laboratory, J.J. Thomson Avenue, Cambridge, CB3 0HE, UK*

²*Kavli Institute for Cosmology, Madingley Road, Cambridge, CB3 0HA, UK*

Accepted XXX. Received YYY; in original form ZZZ

ABSTRACT

We provide a complementary nested sampling analysis for the Atacama Cosmology Telescope lensing data release 6. This allows the quantification of global consistency statistics between ACT lensing and alternative datasets. In the context of flat Λ CDM, we find no inconsistency between ACT, Baryonic Acoustic Oscillations, Planck anisotropies, weak lensing datasets, or NPIPE lensing. As part of our analysis, we also investigate the effect of the prior widths used in the ACT analysis and find that the headline results are quantitatively but not qualitatively affected by the chosen priors. We use both Bayes factors and the suspiciousness statistic to quantify the possibility of tension, and find suspiciousness unsuitable in the case of strong agreement between ACT DR6 and NPIPE. Nested sampling provides a competitive alternative to Metropolis Hastings and we recommend it be used alongside existing analyses. We release the chains and plotting source for the analysis using `anesthetic`.

Key words: methods: statistical – cosmological parameters – gravitational lensing: micro

1 INTRODUCTION

The Atacama Cosmology Telescope gravitational (ACT) lensing map data release 6 (DR6) provides constraints on the parameters of Λ CDM cosmology and its extensions. (Madhavacheril et al. 2023; MacCrann et al. 2023; Qu et al. 2023). Combining ACT DR6 with other datasets, such as Baryonic Acoustic Oscillations (BAO), can provide constraints on cosmological parameters tighter than considering the datasets separately. However, care must be taken when combining measurements. The validity of combining two datasets can be assessed using statistics such as the Bayes factor or *suspiciousness* (Abbott et al. 2018; Handley & Lemos 2019b).

Suspiciousness is a prior-independent measure of the compatibility of two datasets, unlike the Bayes factor which is prior dependent. We use both statistics to quantify the validity of combining the ACT lensing measurements with BAO, the Dark Energy Survey Year 1 (DES-Y1), Planck anisotropy measurements, and NPIPE lensing, in the context of flat Λ CDM.

Our repeat of ACT’s constraints in the $\Omega_m - \sigma_8$ plane is shown in Figure 1(a). While this displays the impressive constraints obtained by combining the ACT lensing measurements with BAO data, it obscures what may be happening in the rest of the parameter space. This is of interest as ACT use informative priors; we investigate the effect of instead using uninformative priors. Neither ACT nor BAO data constrain the Baryonic matter density $\Omega_b h^2$, spectral index n_s , or optical depth τ , so ACT used Gaussian priors centred on the Planck values. This reduces the time taken for the MCMC (Markov Chain Monte Carlo) sampling approach ACT used to reach convergence.

Nested sampling (Skilling 2004) provides an alternative approach to Metropolis-Hastings methods for producing posterior samples as a by-product of computing the Bayesian evidence. Nested sampling has no issue with unconstrained parameters, the posterior samples will correspond to their prior without an unacceptable increase in convergence time. Computing the Bayesian evidence in addition to the posterior is important for model and dataset comparison.

We use `PolyChord` to generate the posterior samples, and perform tension analysis using `anesthetic` (Handley et al. 2015a,b; Handley 2019). `anesthetic` was also used to produce the posterior corner plots.

2 METHODS

2.1 Tools

This work uses the nested sampling tool `PolyChord 1.20.2` to explore the parameter spaces and produce posterior samples. The sampling and modelling framework `Cobaya` (Torrado & Lewis 2019, 2021) provides the interface between the likelihoods, sampler and the Boltzmann code `CAMB 1.4.2.1` (Lewis et al. 2000; Lewis & Bridle 2002; Howlett et al. 2012). We use a modified version of `Cobaya 3.3.1` with improvements to the interface with `PolyChord`¹. All nested sampling runs were performed with 1000 live points. A development version of the recently released `anesthetic 2` was used to create the posterior plots and compute the tension statistics.

* E-mail: ano23@cam.ac.uk

¹ <https://github.com/handley-1ab/cobaya>

2.2 Likelihoods

2.2.1 ACT lensing

Only the ACT DR6 lensing results have so far been published, with a corresponding Cobaya likelihood. This likelihood has four variants: ACT-only or ACT+Planck, each using either the baseline or extended multipole range. We restrict this analysis to the baseline multipole range. There is also an option `lens_only` which must be set to false when combining with any primary CMB measurement.

ACT recommend a minimum set of CAMB settings in their README², these are the settings used here. These are included in appendix A.

2.2.2 NPIPE Planck lensing

To assess the validity of combining ACT and Planck lensing measurements, we also require a separate Planck lensing likelihood. Here we use the NPIPE Planck DR4 likelihoods (Carron et al. 2022a,b). Similarly to the ACT likelihoods, there are versions un-marginalised and marginalised over CMB measurements, which should be used with and without a separate CMB measurement respectively.

Since ACT and NPIPE lensing are measurements of the same sky, they have significant correlation, which means the likelihood corresponding to using both datasets is not the product of the likelihoods for each dataset individually. This is addressed in the ACT likelihood, which we modified to take two sets of cosmological parameters, one for ACT and one for NPIPE. This process is described in more detail in section 2.5.

2.2.3 Planck anisotropies

There are a selection of Planck likelihoods for both low- ℓ ($2 < \ell < 29$) and high- ℓ . Since we are using the NPIPE Planck lensing, it seems appropriate to venture beyond the 2018 Plik likelihoods. For low- ℓ , we use the `click` COMMANDER TT, SRo112 EE likelihoods, and for high- ℓ the NPIPE CamSpec combined TTTEE likelihood (Planck Collaboration et al. 2020a; Pagano et al. 2020; Rosenberg et al. 2022).

CamSpec uses the Planck PR4 (NPIPE) maps released in 2020. The NPIPE maps correspond to approximately 10% tighter parameter constraints compared to the 2018 maps. SRo112 also improves upon the 2018 low- ℓ EE maps by improving the corrections for the nonlinear response of the analogue-to-digital converters of the Planck High Frequency Instrument, reducing the variance by a factor of two for $\ell < 6$, with improvements up to multipoles of 100. The `click` TT likelihood uses the COMMANDER maps.

The ACT analysis did not include any Planck low- ℓ TT maps; COMMANDER is included here for the sake of completeness as it does not dramatically alter parameter values (table B1). We use this for reference contours in posterior plots.

2.2.4 BAO

To break the degeneracies between H_0 and Ω_m , ACT use data from the 6dF and SDSS surveys, specifically 6dFGS, SDSS DR7 Main Galaxy Sample (MGS), BOSS DR12 luminous red galaxies (LRGs) and eBOSS DR16 LRGs (Beutler et al. 2012; Ross et al. 2015; Alam et al. 2021). Only BAO information is included, which requires making a copy of the data files and covariance matrices from the native

Cobaya eBOSS DR16 likelihood, removing the `fsigma8` elements from each, and providing these to a generic Cobaya BAO likelihood. The data files and a copy of the yaml file are included in the cookbook (Ormondroyd et al. 2023).

2.2.5 DES-Y1

The Dark Energy Survey analysed data from cosmic weak lensing shear, galaxy clustering, and galaxy-galaxy lensing (Abbott et al. 2018). Together, they are referred to as 3x2 (the combination of three two-point functions). However, the ACT analysis only uses the weak lensing shear. Here, we consider both the weak lensing shear alone and the full 3x2 suite, labelled here DES-Y1 lensing and DES-Y1 3x2. Cobaya only has access to the Year-1 likelihoods, so we use these here to maintain a level playing field between the datasets.

As part of the changes in preparation for the Euclid telescope (Lau-reijs et al. 2011), Cobaya has introduced limits on the wavenumbers to which CAMB will extrapolate³. In this work we removed these limits, as they prevent DES-Y1 from completing the early part of the nested sampling run where it is still exploring very unlikely regions of the parameter space.

2.3 Priors

ACT use different priors depending on whether they include anisotropy data. Regardless of one's views on prior dependence, the performance of individual datasets should be assessed with the same priors. Neither lensing nor Baryonic Acoustic Oscillations measurements constrain baryonic matter density $\Omega_b h^2$, spectral index n_s , or optical depth to reionisation τ . ACT used informative priors on $\Omega_b h^2$ and n_s centred on the Planck 2018 values (Planck Collaboration et al. 2020b), and fixed $\tau = 0.055$. Note that these Gaussian priors are approximately five times wider than the Planck constraints, which ACT say are "quite conservative". MCMC is very inefficient at exploring these near-flat dimensions, but they pose no additional difficulties for nested sampling. We first repeated the analysis using nested sampling and their informative priors, to check that our posteriors were similar. The priors were then relaxed to match the uniform uninformative ACT priors, including τ . Like ACT, we do not use the informative priors when Planck anisotropies are included.

PolyChord took around two hours to converge using either prior with ACT lensing alone, but slowed slightly to three hours for ACT + BAO with uniform priors due to the extra nuisance parameters associated with the BAO likelihoods. These correspond to around 1-2 CPU hours per live point. We also investigated whether it would have been viable to use MCMC sampling with the uniform prior. We used 9 MCMC chains each parallelised over 8 CPU cores, until the Gelman-Rubin criterion (Gelman & Rubin 1992) falls below $R - 1 = 0.01$. MCMC was always slower than nested sampling, taking an order of magnitude longer to reach convergence using uniform priors, just over ten days for ACT + BAO. Convergence times are listed in table 1. The posterior plots from the MCMC chains were identical to those from nested sampling, so we have not shown them here.

These times were recorded using Python 3.9.12 on the ice-lake partition of the Cambridge Service for Data Driven Discovery (CSD3). MCMC was performed using 72 CPU cores, and nested sampling with $10 \times 76 = 760$ cores. While using ten times more cores may appear to unfairly favour PolyChord, using this many cores with MCMC would just correspond to running ten times as many

² https://github.com/ACTCollaboration/act_dr6_lenslike

³ <https://github.com/CobayaSampler/cobaya/pull/222>

Parameter	Prior	
	Informative	Uniform
$\Omega_c h^2$	[0.005, 0.99]	[0.005, 0.99]
$\Omega_b h^2$	$\mathcal{N}(0.02233, 0.00036^2)$	[0.005, 0.1]
$\ln 10^{10} A_s$	[1.61, 4.0]	[1.61, 4.0]
n_s	$\mathcal{N}(0.96, 0.02^2)$	[0.8, 1.2]
$100\theta_{MC}$	[0.5, 10]	[0.5, 10]
H_0	[40, 100]	[40, 100]
τ	0.055	[0.01, 0.8]

Table 1. Priors for the parameters used in this work. Fixed values are indicated by a single number, uniform priors are denoted by square brackets, and Gaussian priors as $\mathcal{N}(\mu, \sigma^2)$. These priors correspond to those used in the ACT analysis (Madhavacheril et al. (2023)), which themselves follow those of the Planck analyses (Planck Collaboration et al. (2020b)). The informative priors were used by ACT when CMB anisotropy data was not included, since $\Omega_b h^2$, n_s and τ are not constrained by CMB lensing or BAO. Here, we compare the use of both priors to understand the effect of the informative prior on the posteriors of the parameters which are constrained by these datasets. We refer to the two priors as “informative” and “uniform” throughout this text.

chains, as CAMB is not intended to be parallelised beyond around 16 OpenMP processes, which overall would likely take even longer to converge.

These timings will become quickly outdated with new CPUs, improvements to the Boltzmann codes, likelihoods and Python itself, but their relative values should remain consistent with what we find here.

2.4 Quantifying tension between uncorrelated datasets

Cosmological models may be compared via their Bayes factor, calculated using the same dataset. However, here we wish to compare two datasets to assess whether they are in tension. This is usually achieved through the evidence ratio:

$$R = \frac{Z_{AB}}{Z_A Z_B}, \quad (1)$$

where Z_A and Z_B are the Bayesian evidences calculated using datasets A and B respectively, and Z_{AB} is calculated using both datasets jointly. Suspiciousness aims to remove the prior dependence of R . If there are any reasonable priors which reduce this confidence R to below unity, then the two datasets are in tension.

Suspiciousness, coined in Handley & Lemos (2019b), approximately removes the prior dependence from R by dividing it by the ratio of the Kullback-Leiber (KL) divergences between the posterior and the prior of each dataset. Suspiciousness can then be written as the ratio of the expectation values of the log-likelihoods:

$$\log S = \langle \log \mathcal{L}_{AB} \rangle_{\mathcal{P}_{AB}} - \langle \log \mathcal{L}_A \rangle_{\mathcal{P}_A} - \langle \log \mathcal{L}_B \rangle_{\mathcal{P}_B}, \quad (2)$$

where $\langle \log \mathcal{L} \rangle_{\mathcal{P}}$ denotes the average value of (\log) likelihood \mathcal{L} over the posterior distribution \mathcal{P} . In the case that the likelihood is exactly Gaussian, $d - 2 \log S$ has a χ_d^2 distribution, where d is the Bayesian model dimensionality defined in Handley & Lemos (2019a). This is used to calculate the *tension probability*, p , that discordance between the datasets is by chance:

$$p = \int_{d-2 \log S}^{\infty} \chi_d^2(x) dx = \int_{d-2 \log S}^{\infty} \frac{x^{d/2-1} e^{-x/2}}{2^{d/2} \Gamma(d/2)} dx. \quad (3)$$

If $p \lesssim 0.05$ (corresponding to two Gaussian standard deviations) then the datasets are in moderate tension, while $p \lesssim 0.003$ corresponds to their being in strong tension.

2.5 Quantifying tension between correlated datasets

If two datasets have significant correlation, we must include this when comparing the two datasets (Lemos et al. 2020). Equation 1 is really making the following comparison:

$$R = \frac{Z(\text{datasets } A \text{ and } B \text{ fit one universe together})}{Z(\text{datasets } A \text{ and } B \text{ fit one universe each})} = \frac{Z(H_0)}{Z(H_1)}, \quad (4)$$

where H_0 is the null hypothesis that the two datasets are both measurements of the same universe; H_1 is the alternative hypothesis that they are each a measurement of a separate universe with different cosmological parameters. The corresponding suspiciousness then becomes:

$$\log S = \langle \log \mathcal{L}_{H_0} \rangle_{\mathcal{P}_{H_0}} - \langle \log \mathcal{L}_{H_1} \rangle_{\mathcal{P}_{H_1}}. \quad (5)$$

The ACT DR6 lensing likelihood is Gaussian in the data, so the likelihood corresponding to H_1 is:

$$\log \mathcal{L}_{H_1} = \log \mathcal{L}_{H_1 \max} \quad (6)$$

$$- \frac{1}{2} \begin{bmatrix} C_\ell(\theta_A) - D_A \\ C_\ell(\theta_B) - D_B \end{bmatrix}^\top \begin{bmatrix} C_A & C_X \\ C_X^\top & C_B \end{bmatrix}^{-1} \begin{bmatrix} C_\ell(\theta_A) - D_A \\ C_\ell(\theta_B) - D_B \end{bmatrix}.$$

θ_A and θ_B are the parameters corresponding to the two universes, which Cobaya provides to CAMB to calculate the CMB power spectrum $C_\ell(\theta)$. D_A and D_B are the power spectra measured by ACT and NPIPE respectively, C_A and C_B are the correlations within each dataset and C_X are the cross-correlations between the two. The evidence for the alternative hypothesis is calculated by integrating over the doubled parameter space:

$$Z(H_1) = \int \mathcal{L}_{H_1} \pi(\theta_A) \pi(\theta_B) d\theta_A d\theta_B. \quad (7)$$

One can see that $Z(H_1) = Z_A Z_B$ in the case the two datasets are uncorrelated, where the cross-correlations $\Sigma_X = 0$, and we recover the prescription in the previous section. The likelihood for H_0 with a single set of parameters θ can then be obtained by fixing $\theta_A = \theta_B$:

$$\mathcal{L}_{H_0}(\theta) = \mathcal{L}_{H_1}(\theta_A = \theta, \theta_B = \theta), \quad (8)$$

so the evidence for the null hypothesis is:

$$Z(H_0) = \int \log \mathcal{L}_{H_0} \pi(\theta) d\theta. \quad (9)$$

Out of the box, the ACT Cobaya likelihood only requests a single set of C_ℓ s, corresponding to $\log \mathcal{L}_{H_0}$. To compute H_1 , we modified the likelihood to request two sets of C_ℓ s using each half of the doubled parameter space. More detail and the source code is also included in the cookbook (Ormondroyd et al. 2023).

3 RESULTS

Comparing figures 1 (a) and (b), we make the reassuring observation that using uniform priors causes the lensing + BAO 1σ -contours to better fill the intersection between the individual contours of lensing and BAO, compared to using the informative priors. In table 3, we also see that the 1-D S_8 constraint from ACT + BAO has only changed slightly with uniform priors, despite the much weaker constraint on H_0 and the other parameters shown in the corner plot (figure 2).

We calculated Bayes factors and probabilities of chance discordance p for ACT versus BAO, ACT versus DES-Y1, and ACT versus Planck anisotropies. We then also calculated NPIPE versus DES-Y1. Using the uniform prior, we find $p = 30 \pm 4\%$ between ACT and BAO, which increases to $37 \pm 2\%$ with the informative prior. We

Data	Prior	Sampler	Walltime	CPU time	CPU time/chain	CPU time/live point
ACT lensing	informative	MCMC	7h30	570h	63h20	1h15
		PolyChord	1h39	1254h		
	uniform	MCMC	124h	8680h	868h	1h34
		PolyChord	2h04	1575h		
ACT + BAO	informative	MCMC	13h00	988h	110h	1h24
		PolyChord	1h50	1393h		
	uniform	MCMC	247h	18772h	1877h	2h18
		PolyChord	3h02	2299h		

Table 2. Convergence times for ACT lensing and ACT + BAO, using both MCMC sampling and nested sampling with PolyChord, and both informative and uniform priors. MCMC takes over ten times longer to converge with the uninformative priors, long enough that we had concerns they would not converge at all. In contrast, PolyChord only takes around one and a half times longer. In the informative case, the MCMC sampling did use less cpu time, but the parallelisation of nested sampling provides a lower walltime. These timings were taken using Python 3.9.12 on the icelake partition of CSD3, using 76 CPU cores for MCMC, and $10 \times 76 = 760$ cores for PolyChord. These timings will quickly become outdated with new CPUs and improvements to Python speed, but the scaling should remain consistent with what we have found.

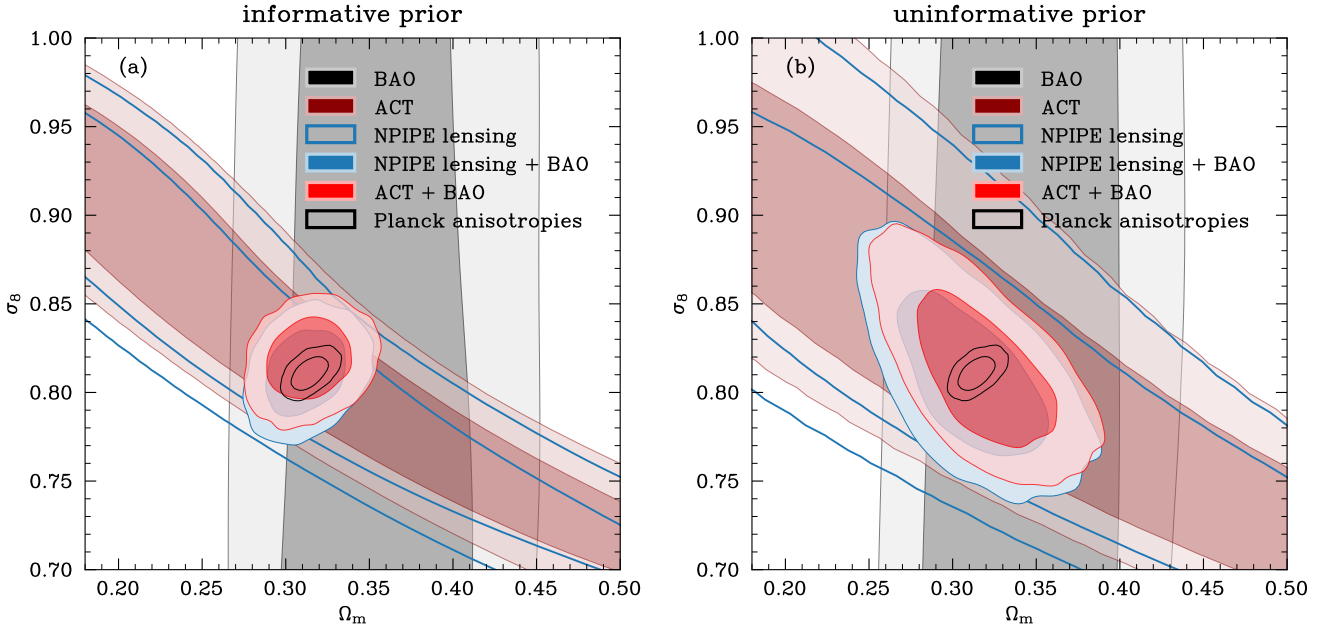


Figure 1. (a) *left:* The amplitude of matter fluctuations σ_8 measured by ACT lensing, BAO, Planck lensing, and Planck CMB anisotropies. These were obtained using PolyChord and the informative priors used in Madhavacheril et al. (2023) on $\Omega_b h^2$, n_s , and fixed τ . This is a repeat of figure 6(a) from that paper. Lensing is degenerate in H_0 and Ω_m ; the latter is broken by BAO. The measurement of σ_8 measured by combining ACT with BAO agrees with NPIPE lensing + BAO, as well as Planck anisotropy measurements. However, it can be seen that the 1σ contours of the combined datasets are not simply the intersection of those of the separate datasets, suggesting further investigation is required. (b) *Right:* Repeat of (a), using uniform priors on all parameters including τ . The ACT + BAO and NPIPE 1σ contours fill those of the separate datasets far less suspiciously.

The Planck anisotropy contours (with uniform priors) are included on both figures for contrast, these include high- l TTTEEE, low- l TT and low- l EE likelihoods.

find almost 100% between ACT and DES-Y1 lensing for both priors, this reduces to around 41% for DES-Y1 3x2. Finally for ACT, we find $p = 85 \pm 5\%$ with Planck anisotropy measurements. Therefore, we conclude that ACT is in tension with neither BAO, DES-Y1, or Planck. We also find NPIPE has slightly greater tension with BAO than ACT, but has a similar lack of tension with DES-Y1 lensing. We find in every case that $\log R > 1$, supporting that these data are not in tension.

Finally, we compared ACT lensing with NPIPE lensing, which required the methods described in section 2.5. For both priors we obtain Bayes factors $\log R > 6$, so we believe they also are not in tension. However, with the uniform prior, we find $p = 100\%$. This is because the lower bound of the p -value integral, $d - 2 \log S$, is negative, and the χ^2 distribution in equation 3 is of course normalised from $[0, \infty)$. This can be interpreted in two ways: lensing alone

does not significantly constrain the Λ CDM parameter space, so the Gaussian approximation used in the derivation of p does not hold well, but also that the agreement between the two is so strong that it falls very deep in the tail of the χ^2 . The Bayes factor makes no such approximations, and is the appropriate measure to use in this case.

A summary of parameter values and tension statistics are given in table 3; a more complete list of parameter values for both are included in appendix B for reference. However, we recommend downloading and creating corner plots of the nested sampling chains to make proper comparisons.

Data	Prior	H_0 (km/s/Mpc)	$S_8 = \sigma_8 \sqrt{\Omega_m/0.3}$	$\log R$	d	$\log S$	p -value
ACT Vs Planck	uniform			7.053 ± 0.264	2.948 ± 0.414	0.988 ± 0.089	$80.3 \pm 5.1\%$
ACT Vs BAO	informative			2.102 ± 0.109	1.162 ± 0.096	0.081 ± 0.035	$37.0 \pm 2.1\%$
	uniform			1.576 ± 0.110	0.610 ± 0.108	0.044 ± 0.037	$29.9 \pm 3.7\%$
ACT Vs DES-Y1 lensing	informative			3.857 ± 0.122	1.261 ± 0.134	0.688 ± 0.046	$98.6 \pm 3.7\%$
	uniform			3.691 ± 0.132	1.796 ± 0.150	1.005 ± 0.052	$99.9 \pm 0.7\%$
ACT Vs DES-Y1 3x2	informative			5.095 ± 0.203	3.881 ± 0.363	0.036 ± 0.089	$41.4 \pm 2.6\%$
	uniform			4.506 ± 0.191	4.219 ± 0.379	-0.020 ± 0.094	$40.2 \pm 2.6\%$
NPIPE Vs BAO	informative			2.131 ± 0.109	1.284 ± 0.096	0.029 ± 0.032	$35.1 \pm 2.0\%$
	uniform			1.188 ± 0.102	0.361 ± 0.109	-0.289 ± 0.036	$11.3 \pm 3.1\%$
NPIPE Vs DES-Y1 lensing	informative			3.861 ± 0.125	0.968 ± 0.139	0.608 ± 0.045	$99.8 \pm 1.3\%$
	uniform			3.635 ± 0.128	1.644 ± 0.139	0.936 ± 0.050	$99.9 \pm 0.8\%$
ACT Vs NPIPE	informative			6.232 ± 0.127	1.996 ± 0.103	0.725 ± 0.032	$76.1 \pm 2.0\%$
	uniform			6.412 ± 0.122	1.703 ± 0.124	1.153 ± 0.042	$100.0 \pm 0.0\%^*$

Table 3. H_0 , S_8 , Bayes' factor, Bayesian model dimensionality, suspiciousness and respective p -values for ACT lensing data combined with Planck anisotropies, BAO, DES-Y1 and Planck NPIPE lensing. “Informative” and “uniform” refer to the priors described in table 1. Only the uniform priors are used with Planck anisotropy measurements. All the p -values are well above 0.05, therefore none of the datasets are in tension with one another. Values of S_8 and H_0 shown are those found using the combined datasets.

Notice that using uninformative priors has made only very slight difference to the S_8 measurement by ACT + BAO.

* Comparing ACT and NPIPE lensing, we find them in strong agreement, but following the $\log S$ prescription we find $p = 100\%$. This is because the lower bound of the p -value integral in 3, $d - 2 \log S$, is negative, and a χ^2 distribution is normalised over $[0, \infty)$. This may be interpreted in two ways: very strong agreement between the two lensing measurements, but also the Gaussian approximation used in the suspiciousness statistic breaking in this case where Λ CDM is not well constrained by CMB lensing alone. The Bayes factor involves no such approximations, and $\log R > 6$ for both informative and uniform priors reassures us that ACT and NPIPE lensing are not in tension.

4 CONCLUSIONS

In this paper, we used nested sampling to generate posterior samples of Λ CDM parameters using the ACT DR6 lensing likelihood. We used both the ACT informative priors and the Planck uniform priors, and presented them on corner plots created using `anesthetic` 2. We find that the suspiciously tight constraints on matter fluctuations combining ACT lensing and BAO become more reasonable with the uninformative Planck priors. Both sets of samples were then used to calculate the suspiciousness statistic between ACT lensing and BAO, DES-Y1, and Planck anisotropies, and we find no substantial evidence for tension with either prior. We also find NPIPE lensing is also not in tension with either BAO or DES-Y1.

We have shown that replacing informative priors with uninformative priors makes a substantial difference to constraints in the $\Omega_m - \sigma_8$ plane. Therefore, we conclude that the informative priors used by ACT were not conservative. We found that uninformative priors added tenfold cost to MCMC sampling convergence time, while nested sampling was not significantly slowed down. Therefore, we recommend that nested sampling and uninformative priors are used in future analyses of the ACT lensing datasets.

As ACT lensing and NPIPE lensing measurements are correlated, quantifying their tension required modifying the ACT likelihood code to use two sets of cosmological parameters, one corresponding to each dataset. We find that the suspiciousness p -value breaks down when comparing two datasets in strong agreement which together do not constrain the parameter space. Therefore, we recommend that comparisons of such datasets are made using Bayes factors.

We also hope to either obtain or create a Cobaya DES-Y3 likelihood so we can make up-to-date comparisons with weak lensing.

ACKNOWLEDGEMENTS

This work was performed using the Cambridge Service for Data Driven Discovery (CSD3), part of which is operated by the University of Cambridge Research Computing on behalf of the STFC

DiRAC HPC Facility (www.dirac.ac.uk). The DiRAC component of CSD3 was funded by BEIS capital funding via STFC capital grants ST/P002307/1 and ST/R002452/1 and STFC operations grant ST/R00689X/1. DiRAC is part of the National e-Infrastructure.

The tension calculations in this work made use of `NumPy` (Harris et al. 2020), `SciPy` (Virtanen et al. 2020), and `pandas` (The pandas development team 2023; McKinney 2010). The plots were produced in `matplotlib`, using the `smploplib` template created by Li (2023).

DATA AVAILABILITY

All the nested sampling chains used in this analysis can be obtained from Ormondroyd et al. (2023). This includes a `Jupyter` notebook demonstrating how we used `anesthetic` to create the figures and compute the tension statistics.

REFERENCES

- Abbott T. M. C., et al., 2018, *Phys. Rev. D*, **98**, 043526
 Alam S., et al., 2021, *Phys. Rev. D*, **103**, 083533
 Beutler F., et al., 2012, *MNRAS*, **423**, 3430
 Carron J., Lewis A., Fabbian G., 2022a, *Phys. Rev. D*, **106**, 103507
 Carron J., Mirmelstein M., Lewis A., 2022b, *J. Cosmology Astropart. Phys.*, **2022**, 039
 Gelman A., Rubin D. B., 1992, *Statistical Science*, **7**, 457
 Handley W., 2019, *The Journal of Open Source Software*, **4**, 1414
 Handley W., Lemos P., 2019a, *Phys. Rev. D*, **100**, 023512
 Handley W., Lemos P., 2019b, *Phys. Rev. D*, **100**, 043504
 Handley W. J., Hobson M. P., Lasenby A. N., 2015a, *MNRAS*, **450**, L61
 Handley W. J., Hobson M. P., Lasenby A. N., 2015b, *MNRAS*, **453**, 4384
 Harris C. R., et al., 2020, *Nature*, **585**, 357
 Howlett C., Lewis A., Hall A., Challinor A., 2012, *J. Cosmology Astropart. Phys.*, **2012**, 027
 Laureijs R., et al., 2011, *arXiv e-prints*, p. arXiv:1110.3193
 Lemos P., Köhlinger F., Handley W., Joachimi B., Whiteway L., Lahav O., 2020, *MNRAS*, **496**, 4647
 Lewis A., Bridle S., 2002, *Phys. Rev. D*, **66**, 103511

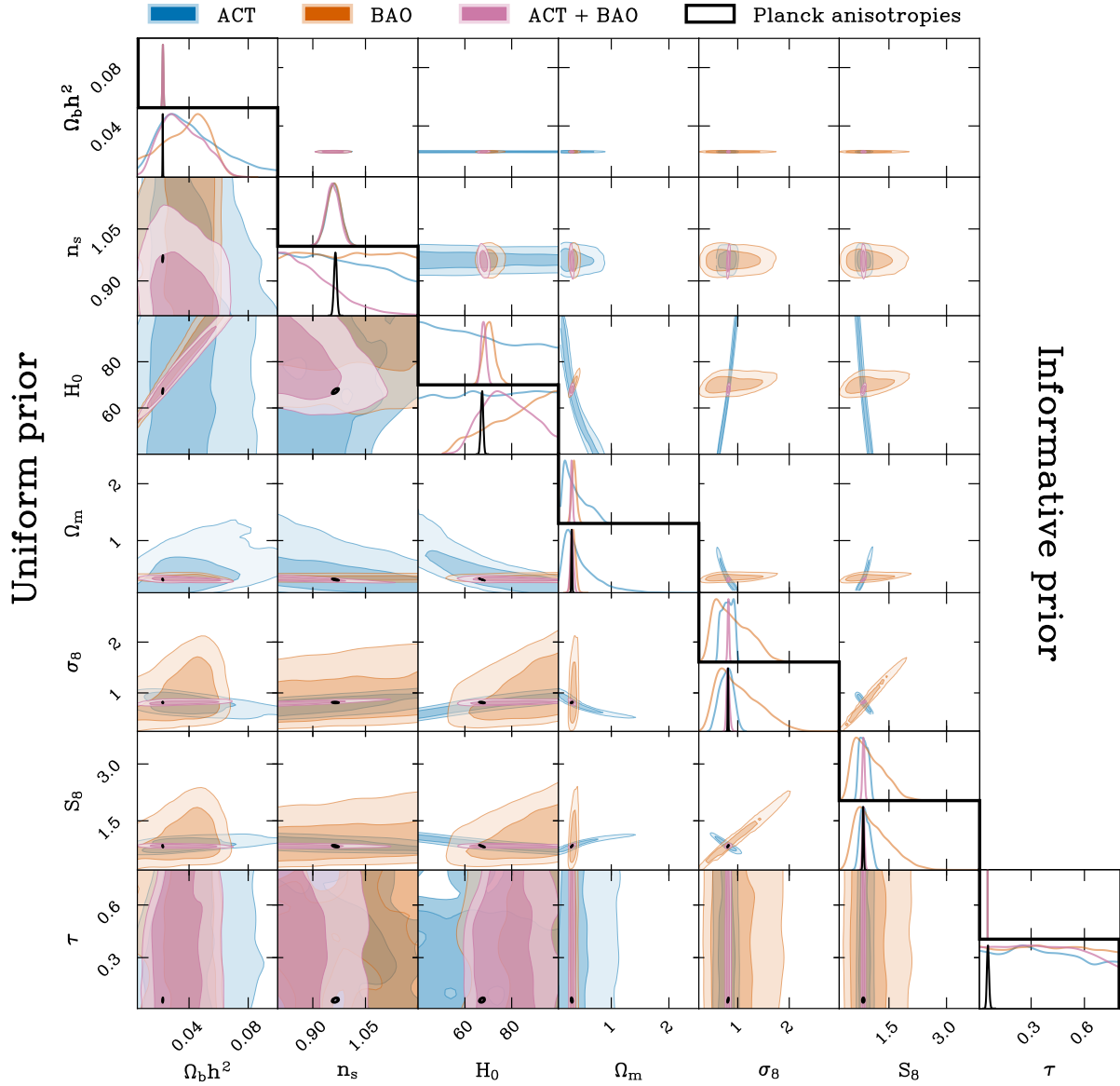


Figure 2. Corner plot comparing cosmological parameter constraints from ACT, BAO, and ACT + BAO, with uninformative and informative priors on $\Omega_b h^2$, n_s and τ . The plots with the informative prior are above the bold diagonal line, those below the diagonal use the uninformative prior. Constraints from Planck anisotropies are also shown for contrast, these only use the uninformative prior. Since τ is fixed, these panels are omitted from the informative prior. As expected, $\Omega_b h^2$, n_s and τ are not constrained by either ACT or BAO, so the uninformative contours occupy most of the prior volume; contrast these with the sparse plots diagonally opposite and the Planck contours, and on S_8 which is well constrained without the need for informative priors. Note also that the Planck constraints on $\Omega_b h^2$, n_s and τ are in fact tighter than the informative prior.

Lewis A., Challinor A., Lasenby A., 2000, *ApJ*, 538, 473
 Li J., 2023, AstroJacobLi/smplotlib: v0.0.9, doi:10.5281/zenodo.8126529, <https://doi.org/10.5281/zenodo.8126529>
 MacCrann N., et al., 2023, *arXiv e-prints*, p. arXiv:2304.05196
 Madhavacheril M. S., et al., 2023, *arXiv e-prints*, p. arXiv:2304.05203
 McKinney W., 2010, in Stéfan van der Walt Jarrod Millman eds, Proceedings of the 9th Python in Science Conference. pp 56 – 61, doi:10.25080/Majora-92bf1922-00a
 Ormondroyd A. N., Handley W., Hobson M., Lasenby A., 2023, Balancing ACT: weighing prior dependency and global tensions of DR6 lensing with other datasets, doi:10.5281/zenodo.10252886, <https://doi.org/10.5281/zenodo.10252886>
 Pagano L., Delouis J. M., Mottet S., Puget J. L., Vibert L., 2020, *A&A*, 635, A99

Planck Collaboration et al., 2020a, *A&A*, 641, A5
 Planck Collaboration et al., 2020b, *A&A*, 641, A6
 Qu F. J., et al., 2023, *arXiv e-prints*, p. arXiv:2304.05202
 Rosenberg E., Gratton S., Efstathiou G., 2022, *MNRAS*, 517, 4620
 Ross A. J., Samushia L., Howlett C., Percival W. J., Burden A., Manera M., 2015, *MNRAS*, 449, 835
 Skilling J., 2004, in Fischer R., Preuss R., Toussaint U. V., eds, American Institute of Physics Conference Series Vol. 735, Bayesian Inference and Maximum Entropy Methods in Science and Engineering: 24th International Workshop on Bayesian Inference and Maximum Entropy Methods in Science and Engineering. pp 395–405, doi:10.1063/1.1835238
 The pandas development team 2023, pandas-dev/pandas: Pandas, doi:10.5281/zenodo.8092754, <https://doi.org/10.5281/zenodo.8092754>

Torrado J., Lewis A., 2019, Cobaya: Bayesian analysis in cosmology, Astrophysics Source Code Library, record ascl:1910.019 (ascl:1910.019)
 Torrado J., Lewis A., 2021, *J. Cosmology Astropart. Phys.*, 2021, 057
 Virtanen P., et al., 2020, *Nature Methods*, 17, 261

APPENDIX A: CAMB SETTINGS

ACT recommend a minimum set of CAMB settings in their README; these are the settings used here in the yaml format used by Cobaya.

```
theory:
  camb:
    stop_at_error: False
    extra_args:
      bbn_predictor: PArthENoPE_880.2_standard.dat
      halofit_version: mead2016
      lens_potential_accuracy: 4
      lmax: 4000
      lens_margin: 1250
      AccuracyBoost: 1
      lSampleBoost: 1
      lAccuracyBoost: 1
      nnu: 3.046
      num_massive_neutrinos: 1
      theta_H0_range:
        - 40
        - 100
```

APPENDIX B: REFERENCE LIST OF PARAMETER CONSTRAINTS

For reference, the following table lists the numeric values of a selection of cosmological parameters for every dataset and combination thereof used in this work.

This paper has been typeset from a \TeX/L\AA\TeX file prepared by the author.

	σ_8	$S_8 = \sigma_8 \sqrt{\Omega_m/0.3}$	Ω_m	H_0 (km/s/Mpc)
informative prior				
ACT	0.801 ± 0.103	0.844 ± 0.104	0.377 ± 0.189	67.2 ± 17.3
ACT (MCMC sampling)	0.810 ± 0.099	0.836 ± 0.100	0.360 ± 0.181	68.5 ± 16.7
BAO	0.895 ± 0.328	0.981 ± 0.384	0.356 ± 0.040	70.5 ± 2.5
DES-Y1 lensing	0.861 ± 0.150	0.789 ± 0.040	0.275 ± 0.100	77.8 ± 12.1
DES-Y1 joint	0.872 ± 0.082	0.791 ± 0.025	0.252 ± 0.038	72.4 ± 7.4
NPIPE	0.814 ± 0.098	0.814 ± 0.102	0.339 ± 0.178	70.7 ± 17.2
ACT + BAO	0.819 ± 0.015	0.837 ± 0.028	0.314 ± 0.016	68.0 ± 1.1
ACT + BAO (MCMC sampling)	0.818 ± 0.015	0.836 ± 0.027	0.314 ± 0.015	68.0 ± 1.1
ACT + DES-Y1 lensing	0.860 ± 0.042	0.790 ± 0.028	0.256 ± 0.034	75.6 ± 7.1
ACT + DES-Y1 joint	0.839 ± 0.031	0.782 ± 0.014	0.262 ± 0.021	71.9 ± 4.5
NPIPE + BAO	0.812 ± 0.016	0.828 ± 0.029	0.312 ± 0.015	67.9 ± 1.1
NPIPE + DES-Y1 lensing	0.850 ± 0.045	0.785 ± 0.031	0.259 ± 0.038	75.2 ± 7.6
ACT + NPIPE	0.810 ± 0.099	0.827 ± 0.100	0.353 ± 0.180	69.3 ± 17.0
uniform prior				
ACT	0.778 ± 0.127	0.878 ± 0.118	0.462 ± 0.301	70.5 ± 17.3
ACT (MCMC sampling)	0.775 ± 0.126	0.880 ± 0.117	0.467 ± 0.299	69.6 ± 17.3
BAO	1.018 ± 0.397	1.098 ± 0.452	0.346 ± 0.038	82.7 ± 12.2
DES-Y1 lensing	0.803 ± 0.151	0.784 ± 0.041	0.314 ± 0.115	82.2 ± 12.2
DES-Y1 joint	0.877 ± 0.075	0.796 ± 0.026	0.250 ± 0.034	83.3 ± 12.9
NPIPE	0.763 ± 0.123	0.871 ± 0.113	0.471 ± 0.305	71.6 ± 17.2
Planck CMB aniso: high- ℓ TTTEEE + low- l EE	0.812 ± 0.006	0.833 ± 0.014	0.316 ± 0.007	67.2 ± 0.5
Planck CMB aniso: above + low- ℓ TT	0.811 ± 0.006	0.830 ± 0.014	0.314 ± 0.007	67.3 ± 0.5
ACT + BAO	0.813 ± 0.029	0.835 ± 0.028	0.318 ± 0.027	78.2 ± 10.0
ACT + BAO (MCMC sampling)	0.813 ± 0.029	0.835 ± 0.028	0.317 ± 0.028	77.4 ± 10.6
ACT + DES-Y1 lensing	0.863 ± 0.045	0.798 ± 0.026	0.259 ± 0.034	79.7 ± 11.9
ACT + DES-Y1 joint	0.859 ± 0.037	0.787 ± 0.015	0.253 ± 0.021	82.9 ± 10.9
ACT + Planck CMB anisotropies	0.813 ± 0.005	0.835 ± 0.010	0.316 ± 0.006	67.2 ± 0.4
NPIPE + BAO	0.809 ± 0.031	0.822 ± 0.030	0.311 ± 0.028	78.5 ± 11.0
NPIPE + DES-Y1 lensing	0.843 ± 0.046	0.794 ± 0.025	0.269 ± 0.035	82.9 ± 11.1
ACT + NPIPE	0.791 ± 0.125	0.858 ± 0.113	0.425 ± 0.277	71.7 ± 17.2

Table B1. σ_8 , S_8 , Ω_m and H_0 values from the datasets used in this paper. The inclusion of low- ℓ CMB anisotropy data only makes a small difference to the mean parameter values, so they are included in the comparison with ACT. Unless specified as MCMC, nested sampling with PoLyChord was used.